PCCP

PAPER

View Article Online
View Journal | View Issue

Cite this: *Phys. Chem. Chem. Phys.*, 2014, **16**, 16642

The calculation of ^{29}Si NMR chemical shifts of tetracoordinated silicon compounds in the gas phase and in solution†

Cong Zhang,[a] Pascal Patschinski,[a] David S. Stephenson,[a] Robin Panisch,[b] Josef Heinrich Wender,[b] Max C. Holthausen[b] and Hendrik Zipse*[a]

Received 22nd April 2014,
Accepted 25th June 2014

DOI: 10.1039/c4cp01736f

www.rsc.org/pccp

Aiming at the identification of an efficient computational protocol for the accurate NMR assessment of organosilanes in low-polarity organic solvents, ^{29}Si NMR chemical shifts of a selected set of such species relevant in organic synthesis have been calculated relative to tetramethylsilane (TMS, **1**) using selected density functional and perturbation theory methods. Satisfactory results are obtained when using triple zeta quality basis sets such as IGLO-III. Solvent effects impact the calculated results through both, changes in substrate geometry as well as changes in the actual shieldings. Spin–orbit (SO) corrections are required for systems carrying more than one chlorine atom directly bonded to silicon. Best overall results are obtained using gas phase geometries optimized at MPW1K/6-31+G(d) level in combination with shielding calculations performed at MPW1K/IGLO-III level in the presence of the PCM continuum solvation model.

Introduction

The measurement of ^{29}Si NMR chemical shifts is exceedingly helpful in elucidating the identity of silicon-containing molecular systems.[1–13] This is not only true for stable reactants and products of well-defined transformations, but also for silicon-based species generated as transient intermediates in the course of a reaction.[14] In this latter case the combination of theoretically predicted and experimentally measured ^{29}Si NMR chemical shifts is particularly helpful, as was amply demonstrated in detailed studies of, for example, silylenes[15] and disilenes.[16] When attempting to follow the course of base-catalyzed silylation reactions of alcohols, which constitute an important protecting group strategy in organic synthesis,[17,18] we were confronted with the appearance of a number of silicon-based species with rather similar chemical shifts in the solution-phase ^{29}Si NMR spectra.[19] With the goal of identifying a computational protocol for the accurate theoretical prediction of the respective chemical shifts in low-polarity organic solvents, we analyze here the performance of strategies based on DFT- and MP2-level calculations.[20–27] Our particular emphasis will be on the effects of geometry optimization, methods for actual shift calculations, the modeling of solvent effects, and the evaluation of relativistic effects.

[a] *Department of Chemistry, LMU München, Butenandtstrasse 5-13, D-81377 München, Germany. E-mail: zipse@cup.uni-muenchen.de; Fax: +49 89 2180 77738*

[b] *Institute of Inorganic Chemistry, Goethe University, Max-von-Laue-Strasse 7, 60438 Frankfurt am Main, Germany. E-mail: max.holthausen@chemie.uni-frankfurt.de; Fax: +49 69 798 29412*

† Electronic supplementary information (ESI) available. See DOI: 10.1039/c4cp01736f

Results and discussion

The effects of geometry optimization

We first investigated the influence of molecular structures optimized using several computationally efficient methods on the quality of ^{29}Si chemical shifts evaluated on these structures at MP2(FULL)/IGLO-III level. These calculations were performed using $SiMe_3Cl$ (**2**) as a model system for silyl chloride reagents used in organic synthesis. Experimentally measured chemical shifts for this system are available in selected solvents at room temperature such as benzene with $\delta(^{29}Si, \mathbf{2}) = +30.21$ ppm,[28] benzene-d_6 with $\delta(^{29}Si, \mathbf{2}) = +30.64$ ppm,[29] toluene-d_8 with $\delta(^{29}Si, \mathbf{2}) = +30$ ppm,[30] and $CDCl_3$ with $\delta(^{29}Si, \mathbf{2}) = +30.7$ ppm.[31] It thus appears that organic solvents of intermediate polarity have only a very limited influence on the ^{29}Si chemical shift in **2**. Using microwave spectroscopy the gas phase Si–Cl bond distance in **2** has been determined in two separate studies as $r(Si–Cl, \mathbf{2}) = 202.2 \pm 5$ pm[32] and 203 pm.[33] In the solid state the Si–Cl bond distance has been determined to be of comparable length at $r(Si–Cl, \mathbf{2}) = 209$ pm,[34] 201.0 pm (0.23 GPa and 296 K),[35] and 208.6 pm (0.1 MPa and 157 K).[36]

The marked dependence of computed chemical shifts on the molecular structure is illustrated in Fig. 1, which displays ^{29}Si chemical shifts calculated for $SiMe_3Cl$ (**2**) at MP2(FULL)/IGLO-III level employing structures optimized at various levels of theory in combination with the 6-31+G(d) basis set (the results

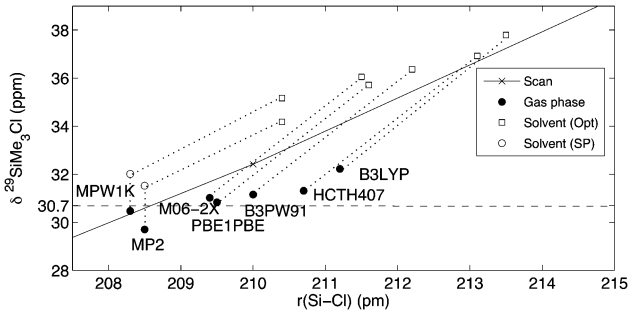

Fig. 1 Calculated $\delta(^{29}Si)$ values for $SiMe_3Cl$ (**2**) (MP2: solid circles and PCM/MP2: empty symbols; IGLO-III basis set) using molecular structures optimized at various levels of theory using the 6-31+G(d) basis set. Dashed line: experimental value in $CDCl_3$; solid line: relaxed scan along the Si–Cl bond (gas phase, MPW1K structures). Empty circles: PCM/MP2 shifts on gas phase structures; empty squares: PCM/MP2 shifts on solution-phase geometries (all solvent calculations: $CHCl_3$, UAHF radii).

obtained from MP2(FULL)/IGLO-III geometry optimizations are included as a reference). ^{29}Si chemical shifts evaluated for various points along a relaxed scan (MPW1K/6-31+G(d) structures) of the Si–Cl distance in **2** from 200 to 300 pm (solid line in Fig. 1) show an almost linear dependence with larger Si–Cl distances leading to systematically higher chemical shifts. This trend is also visible in the $\delta(^{29}Si)$ data evaluated on molecular structures fully optimized with different methods in the gas phase (Fig. 1, solid circles): the shortest Si–Cl bond distances (about 208.5 pm) are obtained in MPW1K and MP2(FC) optimizations, while the other density functionals tested yield longer Si–Cl bonds reaching 211 pm obtained with the B3LYP hybrid functional. The shift values calculated for these gas phase geometries at MP2(FULL)/IGLO-III level vary by approx. 2 ppm from +29.7 to +32.0 ppm. As detailed further below, use of the PCM solvent model for structure optimization (Fig. 1, empty squares) leads to systematically longer Si–Cl bonds and, correspondingly, to systematically higher $\delta(^{29}Si)$ values, with larger deviations from experiment for the cases tested.

We further explored whether chemical shift predictions can be improved through the use of more sophisticated basis sets in gas phase geometry optimizations for selected Pople-style and correlation consistent (cc) basis sets (Table 1). Use of the systematically developed cc basis sets results in a systematic decrease of Si–Cl bond distances in the order cc-pVDZ, cc-pVTZ, and cc-pVQZ, irrespective of the theoretical method used. This directly impacts the ^{29}Si chemical shift calculations performed at MP2(FULL)/IGLO-III level, where shorter Si–Cl bonds are again observed to yield lower shift values. A comparable trend is not observed for Pople-style basis sets of double- and triple-zeta quality. Among all quantum mechanical methods the MP2(FC) level is most strongly affected by these variations. Taking the MP2(FC)/cc-pVQZ structure as reference, the best agreement is observed at the MPW1K/6-31+G(d) level, which was therefore chosen for all subsequent geometry optimizations.

Theoretical methods for chemical shift calculations

Chemical shift calculations at MP2(FULL)/IGLO-III level are quite challenging for larger molecular systems and an effort has therefore been made to identify more economical approaches. Table 2 displays ^{29}Si shift values for $SiMe_3Cl$ (**2**) computed with selected combinations of methods and basis sets based on the MPW1K/6-31+G(d)-optimized geometry. Compared to the experimental value of $\delta(^{29}Si, \mathbf{2}) = +30.7$ ppm[31] largest deviations are found for the 6-311++G(2d,2p)[26] basis set, while the def2-TZVP,[37,38] cc-pVTZ,[39] and IGLO-III[40] triple zeta basis sets yield generally better results. The quadruple zeta pcS-3 basis set specifically developed for NMR calculations[41] performs as well as IGLO-III, but its use is computationally significantly more demanding. We note that second-order perturbation theory in its canonical (MP2) or local (LMP2) variants perform best, closely followed by the HCTH407[42] and MPW1K[20] hybrid functionals. Interestingly, the DF-LMP2/IGLO-III[43] calculations closely reproduce the much more costly MP2(FULL)/IGLO-III calculations, which we chose as reference method for ^{29}Si chemical shift calculations. The worst performer found here is clearly the M06-2X[44] functional, which responds more sensitively to the individual basis set design than any other method listed in Table 2. The deviations of MPW1K and HCTH407 are comparable to those of the MP2 methods and the performance of these two methods is better than that of the other DFT methods tested here.

Solvent effects

The experimental reference shift data for $SiMe_3Cl$ (**2**) has been determined in apolar organic solvents such as $CDCl_3$ or benzene. As a first straightforward approach to account for solvent effects we performed shift calculations in combination with the

Table 1 Influence of basis set choice on the gas phase geometry optimized with various methods and the gas phase ^{29}Si chemical shift of **2** (evaluated at MP2(FULL)/IGLO-III level)

	PBE1PBE		MPW1K		M06-2X		MP2(FC)	
Basis set	r(Si–Cl) (pm)	$\delta(^{29}Si)$ (ppm)	r(Si–Cl) (pm)	$\delta(^{29}Si)$ (ppm)	r(Si–Cl) (pm)	$\delta(^{29}Si)$ (ppm)	r(Si–Cl) (pm)	$\delta(^{29}Si)$ (ppm)
6-31+G(d)	209.5	+30.84	208.3	+30.32	209.4	+31.02	208.5	+29.70
6-31+G(2d,p)	209.6	+31.81	208.5	+31.37	209.5	+31.90	210.2	+32.60
6-31++G(2d,p)	209.6	+31.82	208.5	+31.38	209.5	+31.92	210.3	+32.63
6-31++G(2df,p)	208.9	+30.90	207.8	+30.43	211.4	+34.14	208.5	+30.44
6-311++G(2d,p)	209.4	+31.82	208.3	+31.31	209.3	+31.90	209.9	+32.30
cc-pVDZ	211.2	+32.98	210.2	+32.63	211.1	+33.16	210.7	+31.83
cc-pVTZ	209.1	+31.23	208.1	+30.81	209.1	+31.39	208.6	+30.79
cc-pVQZ	208.5	+30.77	207.6	+30.36	208.5	+30.92	207.8	+30.24

Table 2 Calculated $\delta(^{29}Si)$ chemical shifts for **2** using different theoretical methods and basis sets[a]

Method[b]	6-311++G(2d,2p)	Def2-TZVP	cc-pVDZ	cc-pVTZ	cc-pVQZ	pcS-3	IGLO-III
HCTH407	+35.00	+32.37	+32.63	+32.91	+26.37	+31.94	+31.40
B3LYP	+36.37	+34.29	+34.13	+34.14	+27.60	+33.44	+32.94
B3PW91	+36.84	+34.92	+35.31	+34.64	+28.78	+34.15	+33.66
PBE1PBE	+36.56	+34.68	+35.35	+34.83	+29.37	+33.93	+33.31
MPW1K	+34.83	+33.06	+33.89	+33.59	+28.09	+32.44	+31.88
M06-2X	+42.67	+38.10	+38.85	+31.00	+36.82	+35.64	+37.24
DF-LMP2	+33.05	+31.47	+31.36	+33.09	+29.55	+30.25	+28.40
MP2(FULL)	+33.65	+31.92	+30.71	+32.54	+28.59	+31.31	+30.32

[a] Geometries optimized with MPW1K/6-31+G(d). [b] Method used for NMR chemical shift calculations.

polarizable continuum model (PCM) for chloroform at PCM/MP2(FULL)/IGLO-III level based on the MPW1K/6-31+G(d) gas-phase geometry, which leads to downfield shifts of the ^{29}Si signal in $SiMe_3Cl$ (**2**) by 1.5–2.0 ppm relative to the gas phase value (+30.32 ppm), depending on the particular PCM variant employed (Table 3). An additional downfield shift of the same magnitude is obtained upon inclusion of the polarizable continuum also for geometry optimization at PCM/MPW1K/6-31+G(d) level owing to the elongated Si–Cl bond present in the optimized structure (Table 3). From a glance at the data compiled in Table 3 it is apparent that the particular choice of the atomic radii used to construct the solute cavity in the PCM calculations has only a minute influence on structures and chemical shifts.

A more detailed picture is presented in Fig. 1 above, where the PCM/MP2(FULL)/IGLO-III shift data using the gas-phase geometries (empty circles) and the solution-phase geometries (empty squares) for selected hybrid DFT methods are shown. Taking the MPW1K/6-31+G(d) gas phase geometries as an example, we can see that the PCM(UAHF)/MP2(FULL)/IGLO-III shifts are 1.7 ppm larger as compared to the gas phase MP2(FULL)/IGLO-III shifts. This is also found for all other methods used for geometry optimization. Reoptimizing the geometry of $SiMe_3Cl$ (**2**) in the presence of the PCM reaction field leads to elongation of the Si–Cl bond, which at PCM/MPW1K/6-31+G(d) level reaches up to 210.4 pm. This geometrical change is accompanied by a downfield shift in the ^{29}Si resonance to +35.0 ppm. This is found in a very similar manner also for all other methods used for geometry optimization and we may thus conclude that the PCM continuum solvation model impacts ^{29}Si shift calculations in a significant way through changes in the molecular structure.

Table 3 Influence of continuum solvation models on ^{29}Si chemical shift calculations (PCM/MP2(FULL)/IGLO-III) for $SiMe_3Cl$ (**2**)

	Gas-phase structure[a]		Solution-phase structure[b]	
	r(Si–Cl) (pm)	$\delta(^{29}Si)$ (ppm)	r(Si–Cl) (pm)	$\delta(^{29}Si)$ (ppm)
PCM(UFF)	208.4	+31.80	210.19	+34.34
PCM(UAHF)	208.4	+32.15	210.40	+35.00
PCM(UAKS)	208.4	+32.15	210.40	+35.00
SMD	208.4	+32.28	210.48	+35.22

[a] Optimized at MPW1K/6-31+G(d) level. [b] Optimized in $CDCl_3$ with different solvation models at MPW1K/6-31+G(d) level.

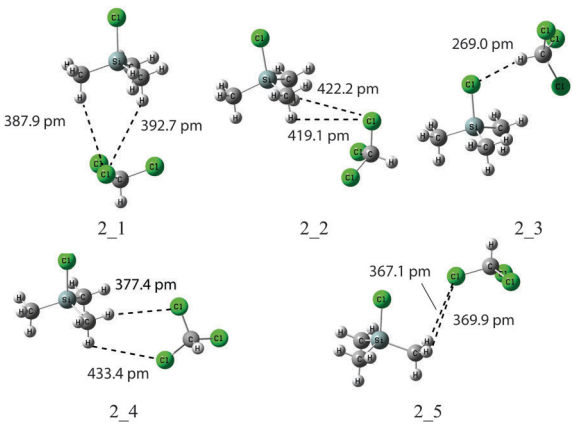

Fig. 2 Structures of $SiMe_3Cl$ (**2**) complexed to $CHCl_3$ obtained at MPW1K/6-31+G(d) level in the gas phase (dashed lines show shortest contacts between solvent and solute molecules).

Effects of explicit solvation were subsequently explored for complexes of $SiMe_3Cl$ (**2**) with one molecule of $CHCl_3$. A number of minima were identified in MPW1K/6-31+G(d) geometry optimizations (Fig. 2). The longest Si–Cl bond with 209.5 pm (and thus the largest downfield shifted ^{29}Si signal) is found for solute–solvent complex **2_3**, in which the chlorine atom of $SiMe_3Cl$ forms a hydrogen bond to chloroform (Table 4). In terms of gas phase free energies ΔG_{298} structure **2_3** is not the most stable conformer, but is 7 kJ mol^{-1} less stable than the best structure **2_1**. Due to only weak interactions between the methyl groups of

Table 4 ^{29}Si chemical shifts for complexes **2_1–2_5** of $SiMe_3Cl$ (**2**) with one chloroform molecule at MP2(FULL)/IGLO-III//MPW1K/6-31+G(d) level (bond distances are in pm, free energies ΔG_{298} are in kJ mol^{-1} and chemical shifts are in ppm)

	Gas phase			Solution phase[a]		
	r(Si–Cl)	ΔG_{298}	$\delta(^{29}Si)$	r(Si–Cl)	ΔG_{298}	$\delta(^{29}Si)$
2_1	208.6	0.00	+30.70	210.50	1.02	+35.09
2_2	208.6	0.99	+30.89	210.50	3.02	+35.43
2_3	209.5	7.01	+33.81	210.70	0.00	+36.24
2_4	208.5	7.44	+30.69	210.40	1.29	+35.16
2_5	208.7	7.91	+31.28	210.40	2.06	+35.06
Ave[b]			+30.88			+35.52

[a] Solvent effects calculated at PCM(UAHF)/MP2(FULL)/IGLO-III//MPW1K/6-31+G(d) level. [b] $\delta(^{29}Si)$ shift calculated as Boltzmann average, for detail see ESI.

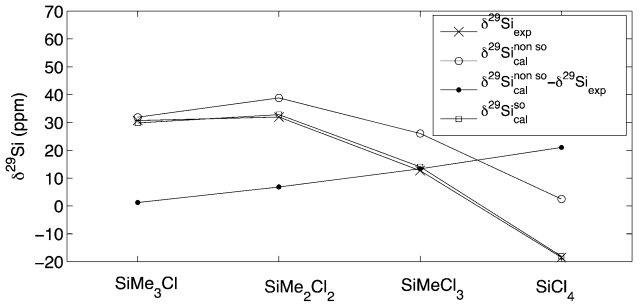

Fig. 3 Comparison between experimentally measured and theoretically calculated shift values at MPW1K/IGLO-III//MPW1K/6-31+G(d) level for alkylchlorosilanes $SiMe_{4-x}Cl_x$ with x = 1–4. SO corrections are obtained from ZORA-SO-PBE0/TZ2P single-point calculations. Geometries are obtained at MPW1K/6-31+G(d) level in gas phase.

2 and chlorine atoms of the solvent molecule, the Si–Cl distance in structure **2_1** is hardly different from that of **2** alone. After Boltzmann averaging, $\delta(^{29}Si)$ is only +0.18 ppm higher than the experimental result. In solution phase, the most stable structure is **2_3**. The continuum solvation model increases the Si–Cl distance and also reduces the energy gap between different conformers. With the PCM solvent model $\delta(^{29}Si)$ values are 5 ppm higher than the experimental value. We thus have to conclude that, at least for model system **2**, the gas phase predictions are significantly closer to the solution phase experiment as compared to solution-phase calculations based on a combined implicit–explicit solvent model.

Spin–orbit corrections for chlorosilanes

^{29}Si Chemical shifts calculated at MPW1K/IGLO-III//MPW1K/6-31+G(d) level for the $SiMe_{4-x}Cl_x$ compounds show a systematic deviation between theoretically calculated and experimentally measured shift data (Fig. 3). That the deviations are systematic in nature can readily be seen from the good linear correlation between the actual deviation and the number of chlorine atoms (Fig. 3).[15] The importance of heavy-atom-induced spin–orbit (SO) effects for nuclear magnetic shifts of group 14 element halides have been highlighted by several groups.[45–50] According to these earlier reports, the experimentally observed normal halogen dependence (NHD), *i.e.* the characteristic high-field shift of the nucleus bound directly to the halogen substituents with increasing atomic number of the halogen, is mainly a result of spin–orbit effects. In these studies it was found that shifts calculated with the inclusion of SO effects agree significantly better with the experiment than their non-relativistic counterparts.

We evaluated contributions of relativistic spin–orbit effects to the nuclear magnetic shielding constants for the series of $SiMe_{4-x}Cl_x$ compounds employing the two-component zeroth-order regular approximation (ZORA)[51,52] formalism, as implemented in ADF. The SO correction per chloro-substituent increases monotonously from approximately −2 ppm ($SiMe_3Cl$) to −3 ppm for $SiMe_2Cl_2$, −4 ppm for $SiMeCl_3$, and −5 ppm for $SiCl_4$. In line with the discussion of Kaupp *et al.* on SO-induced heavy-atom effects on NMR chemical shifts,[47] this trend can readily be explained based on the analogy to the Fermi-contact

Table 5 The ^{29}Si NMR chemical shifts of selected chemical species

	System	δ_{exp}[a] (ppm)	δ_{cal}^{gas}[b] (ppm)	δ_{cal}^{gas+so}[c] (ppm)	δ_{cal}^{sp+so}[d] (ppm)	δ_{cal}^{opt+so}[e] (ppm)
2	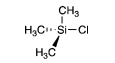	+30.70 ($CDCl_3$)[31]	+31.92	+29.82	+31.90	+34.90
3	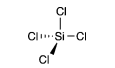	−18.50 ($CDCl_3$)[15]	+2.49	−18.11	−18.05	−18.13
4	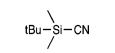	−1.57 ($CDCl_3$)	−5.39	−5.19	−3.01	−1.15
5	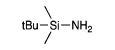	+8.40 (C_6D_6)[55]	+8.97	+8.57	+8.18	+10.41
6	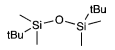	+9.91 ($CDCl_3$)	+11.59	+10.79	+11.21	+12.78
7	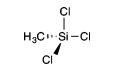	+12.70 ($CDCl_3$)	+26.04	+14.04	+15.30	+16.53
8	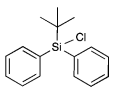	+12.86 ($CDCl_3$)	+16.12	+14.42	+14.73	+15.22
9	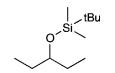	+15.54 ($CDCl_3$)	+17.07	+16.37	+16.88	+18.16
10	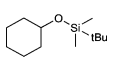	+15.80 ($CDCl_3$)	+17.40	+16.60	+17.28	+18.51
11	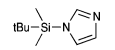	+17.08 ($CDCl_3$)	+16.41	+16.01	+17.13	+19.06
12	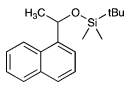	+18.42 ($CDCl_3$)	+21.10	+20.40	+20.68	+21.01
13	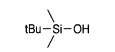	+20.34 ($CDCl_3$)	+19.48	+19.08	+19.09	+20.10
14	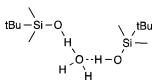	+20.39 ($CDCl_3$)	+17.69	+17.09	+17.84	+18.70
15	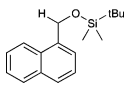	+20.58 ($CDCl_3$)	+21.46	+20.66	+20.95	+18.51
16	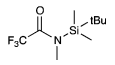	+26.69 ($CDCl_3$)	+22.95	+22.55	+23.36	+24.16
17	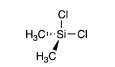	+32.00 ($CDCl_3$)[3]	+38.81	+32.81	+35.13	+37.66
18	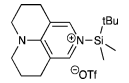	+32.16 ($CDCl_3$)	+35.70	+35.30	+36.18	+34.47
19	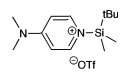	+33.25 ($CDCl_3$)	+38.44	+37.94	+36.40	+37.00
20	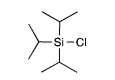	+35.89 ($CDCl_3$)	+36.81	+35.31	+37.13	+39.80
21	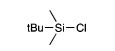	+36.09 ($CDCl_3$)	+37.78	+35.78	+37.62	+39.98
22	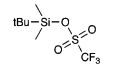	+43.71 ($CDCl_3$)	+44.50	+44.00	+46.55	+51.65
23	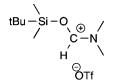	+45.21 ($CDCl_3$)	+51.41	+50.81	+49.83	+49.12

Table 5 (*continued*)

System	δ_{exp}[a] (ppm)	δ_{cal}^{gas}[b] (ppm)	δ_{cal}^{gas+so}[c] (ppm)	δ_{cal}^{sp+so}[d] (ppm)	δ_{cal}^{opt+so}[e] (ppm)
24	+45.96 ($CDCl_3$)	+43.30	+42.70	+43.68	+48.94

[a] Experimentally measured $\delta_{exp}(^{29}Si)$ values for all systems. The solvent is given in parenthesis. [b] $\delta_{cal}^{gas}(^{29}Si)$ chemical shift in gas phase using gas phase structure at MPW1K/IGLO-III//MPW1K/6-31+G(d) level. [c] $\delta_{cal}^{gas+so}(^{29}Si)$ gas phase chemical shift with added Boltzmann-weighted SO corrections. SO corrections are obtained at ZORA-SO-PBE0/TZ2P level in gas phase. [d] $\delta_{cal}^{sp+so}(^{29}Si)$ chemical shifts are calculated with PCM(UAHF)/MPW1K/IGLO-III(+ZORA-SO)//MPW1K/6-31+G(d). Boltzmann-averaged SO corrections are calculated at ZORA-SO-PBE0/TZ2P in gas phase based on gas phase structures. [e] $\delta_{cal}^{opt+so}(^{29}Si)$ chemical shifts are calculated with PCM(UAHF)/MPW1K/IGLO-III//PCM/UAHF-MPW1K/6-31+G(d) level and corrected with Boltzmann-weighted SO corrections at ZORA-SO-PBE0/TZ2P level based on gas phase geometries. For more detailed information on the SO corrections see ESI.

mechanism of spin–spin coupling. The increasing involvement of valence silicon s-type orbitals in the bonding orbitals to the chloro-substituents results in larger SO contributions in the series from $SiMe_3Cl$ to $SiCl_4$.[53] Aside from the chlorine count there is only a rather limited influence of other silicon substituents on the magnitude of the SO corrections. A SO correction of around -2 ± 0.5 ppm per chlorine substituent will thus be typical for different chloromonosilanes (see also Table 5). For systems with more than one conformer, Boltzmann-weighted SO corrections are close to the SO-correction for the most stable conformer.[54]

^{29}Si chemical shifts for larger molecular systems

^{29}Si chemical shifts for a larger group of "typical" systems are collected in Table 5 and graphically shown in Fig. 4. Already the calculation of gas phase ^{29}Si chemical shifts at MPW1K/IGLO-III//MPW1K/6-31+G(d) level provides a rather accurate agreement with experimental results obtained in low polarity organic solvents with R^2 = 0.872 and MD = 2.54 ppm (panel (a) in Fig. 4). The largest deviations occur for systems containing more than one chlorine atom directly attached to silicon, and inclusion of SO-corrections evaluated at ZORA-SO-PBE0/TZ2P single point level improves correlation with experiment significantly for the entire dataset to R^2 = 0.978 and MD = 0.18 ppm (compare panel (a) and (b) in Fig. 4). Best theoretical predictions are then obtained through shielding calculations in the presence of the PCM continuum solvation model with gas phase structures and including the SO corrections. It is remarkable to see that the correlation for this approach based on gas phase structures (R^2 = 0.984, MD = 0.97 ppm) is even slightly better as compared to the approach based on solution-phase structures with R^2 = 0.983 and MD = 2.34 ppm (compare panel (c) and (d) in Fig. 4). Performing the actual shielding calculations with different functionals such as HCTH407 or with the local DF-LMP2 method lead to no further systematic improvement (see ESI† for details).

Chemical shifts for ion pairs

Chemical shift calculations for the ion pair intermediates **18**, **19**, **23**, and **24** included in Table 5 are somewhat less accurate as compared to all other systems at the MPW1K/IGLO-III-(+ZORA-SO)//MPW1K/6-31+G(d) level. This may, in part, be due to significantly larger solvent effects for these polar species as well as their rather large conformational flexibility. How the

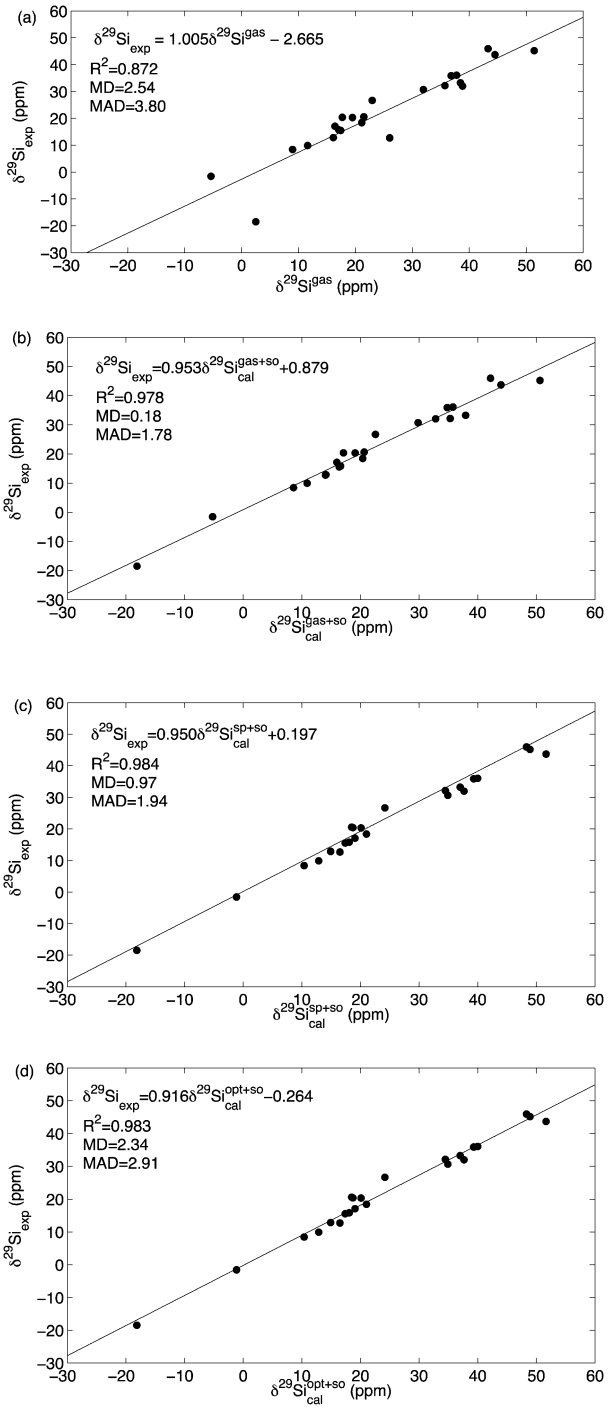

Fig. 4 Theoretically calculated *vs.* experimentally measured ^{29}Si chemical shifts for the data set collected in Table 5. (a) $\delta(^{29}Si)$ calculated at MPW1K/IGLO-III//MPW1K/6-31+G(d) level. (b) $\delta(^{29}Si)$ calculated at MPW1K/IGLO-III(+ZORA-SO)//MPW1K/6-31+G(d). (c) $\delta(^{29}Si)$ calculated at PCM(UAHF)/MPW1K/IGLO-III(+ZORA-SO)//MPW1K/6-31+G(d) level using gas phase structures. (d) $\delta(^{29}Si)$ calculated at PCM(UAHF)/MPW1K/IGLO-III(+ZORA-SO)//PCM(UAHF)MPW1K/6-31+G(d) level using solution phase structures.

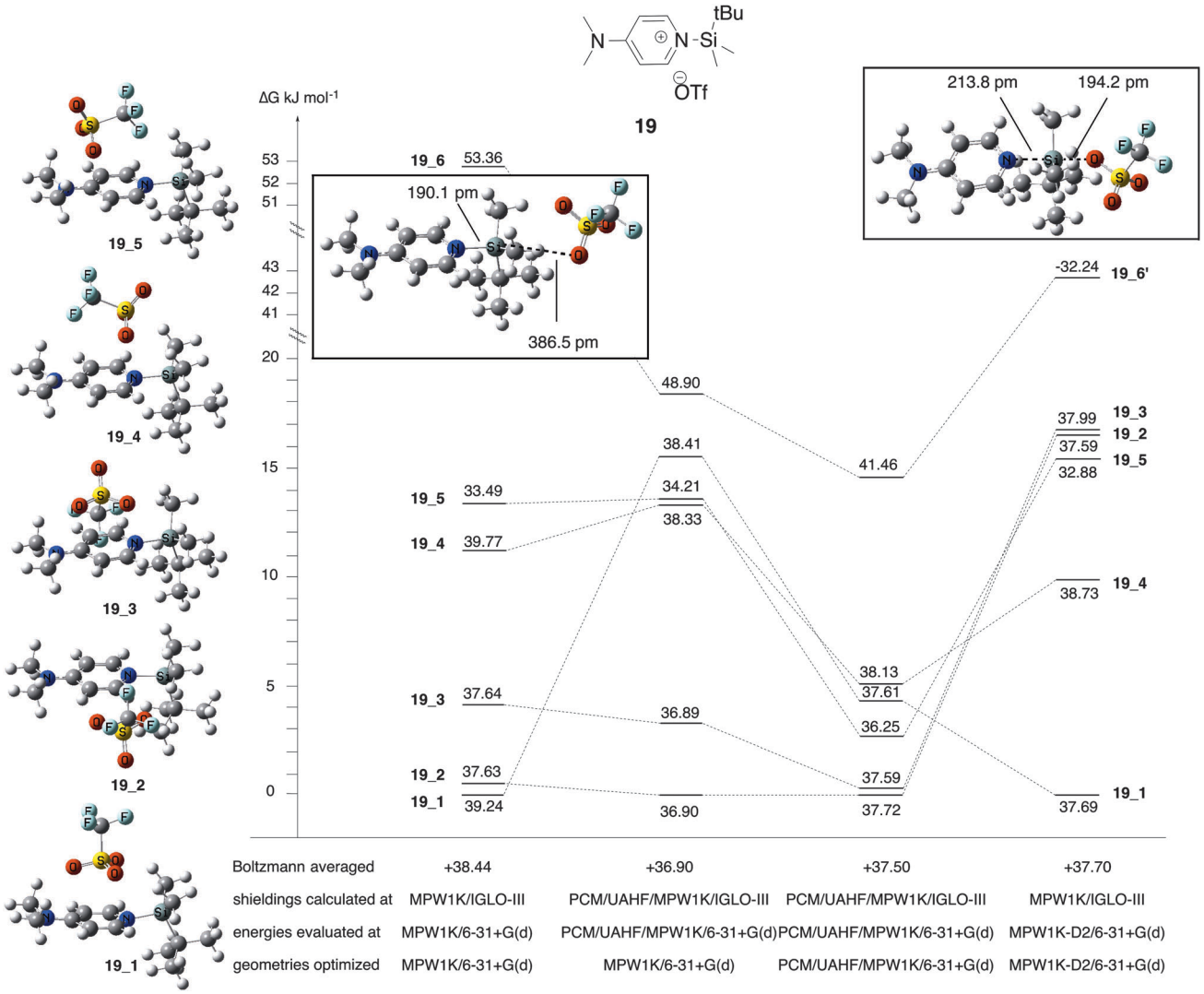

Fig. 5 Relative free energies and chemical shifts of individual conformers of ion pair system **19** at different theory levels.

latter actually impacts chemical shift calculations is illustrated in detail in Fig. 5 for silylpyridinium ion pair **19**, whose experimentally measured ^{29}Si chemical shift amounts to +33.25 ppm in chloroform. For ion pairs, which have more than one conformer, chemical shifts are evaluated by Boltzmann averaging over individual conformers based on their relative free energies. When using gas-phase free energies the structures with the largest molecular dipole moment make the smallest contribution to the Boltzmann average due to their high relative energies (Table 6). In solution, however, these structures lead to the largest solvation energies: the dipole moment of conformer **19_1** is comparatively low at 10.30 D (MPW1K/6-31+G(d) level) and thus has the smallest solvation energy of −81.50 kJ mol^{-1} (gas-phase geometry). Conformers **19_4** and **19_5** have slightly larger dipole moments and also slightly larger solvation energies around −96 kJ mol^{-1}. Conformer **19_6** has the largest dipole moment at 23.93 D, leading to a rather large solvation energy of −131.50 kJ mol^{-1} (gas phase geometry) or −162.72 kJ mol^{-1} (solution phase geometry). As a consequence of these variations in solvation energies, relative free energies in solution (ΔG^{opt}) are significantly smaller as compared to the gas phase. Despite these large changes in relative energies, the actual ion pair structure shows rather little change in gas-phase *vs.* solution-phase geometry optimization as exemplified for the Si–N bond distance (Table 6). This can also be stated for the electronic character of these ion pairs as characterized by the triflate ion charge, which assumes values between −0.94 and −0.96 for the best conformers **19_1** and **19_2** in gas-phase as well as in solution (Table 6).

The largest effects are observed for ion pair **19_6**, whose structure also depends significantly on the chosen level of theory in the gas phase: geometry optimization at MPW1K/6-31+G(d) level leads to the structure shown as "**19_6**" in Fig. 5, which can be characterized as a true ion pair with a comparatively long (387 pm) distance between silicon atom and triflate counter ion. Reoptimization with the same functional and added dispersion corrections (MPW1K-D2/6-31+G(d)) leads to a structure best described as pentacoordinated silicon intermediate (termed **19_6′**) with a much shorter Si–O(triflate)

Table 6 Relative free energies, structural and charge parameters, and ^{29}Si chemical shifts for individual conformational isomers of ion pair **19**. Charge parameters have been obtained from the NBO analysis[56]

Level for free energy calculation		19_1	19_2	19_3	19_4	19_5	19_6
MPW1K/6-31+G(d)//MPW1K/6-31+G(d)	μ (Debye)	10.30	17.27	17.36	13.16	14.39	23.93
	ΔG (kJ mol^{-1})	0.00	0.67	4.01	11.81	13.35	52.89
	r(Si–N) (pm)	184.3	184.9	184.9	184.7	182.9	190.1
	q(OTf)	−0.96	−0.94	−0.94	−0.95	−0.96	−0.95
	δ(^{29}Si) (ppm)	+39.24	+37.63	+37.64	+39.77	+33.49	+53.36
PCM/UAHF/MPW1K/6-31+G(d)//MPW1K/6-31+G(d)	ΔG^{sp}_{solv} (kJ mol^{-1})	−81.5	−97.65	−97.86	−95.60	−96.86	−131.50
	ΔG (kJ mol^{-1})	15.54	0.00	3.13	13.20	13.47	18.23
	r(Si–N) (pm)	184.3	184.9	184.9	184.7	182.9	190.1
	q(OTf)	−0.96	−0.95	−0.95	−0.96	−0.97	−0.96
	δ(^{29}Si) (ppm)	+38.41	+36.90	+36.89	+38.33	+34.21	+48.90
PCM/UAHF/MPW1K-6-31+G(d)//PCM/UAHF/MPW1K-6-31+G(d)	ΔG^{opt}_{solv} (kJ mol^{-1})	−125.81	−119.41	−119.79	−133.05	−141.04	−162.72
	ΔG (kJ mol^{-1})	4.31	0.00	0.29	5.10	2.69	14.51
	r(Si–N) (pm)	184.4	184.5	184.4	184.5	184.2	186.0
	q(OTf)	−0.98	−0.97	−0.97	−0.99	−0.99	−0.98
	δ(^{29}Si) (ppm)	+37.61	+37.72	+37.59	+38.13	+36.25	+41.64
MPW1K-D2/6-31+G(d)//MPW1K-D2/6-31+G(d)	ΔG (kJ mol^{-1})	0.00	16.54	16.76	9.91	15.39	42.78
	r(Si–N) (pm)	183.0	183.5	183.2	183.2	181.6	213.8
	q(OTf)	−0.95	−0.94	−0.94	−0.95	−0.95	−0.78
	δ(^{29}Si) (ppm)	+37.69	+37.59	+37.99	+38.73	+32.88	−32.24

distance of 194 pm and a largely changed ^{29}Si chemical shift of −32.24 ppm.[57] More importantly, the very different chemical shift for pentacoordinate structure **19_6′** clearly supports the assignment of the experimentally detected ion pair species as systems with tetracoordinate silicon atoms. The ''collapse'' of the ion pair structure to a pentacoordinated intermediate upon geometry optimization at MPW1K-D2/6-31+G(d) level has only been observed for conformer **19_6** and not for any of the other (low-energy) conformers.

Conclusions

Calculated ^{29}Si chemical shifts of (chloro)organosilanes depend strongly on structural details of the respective systems. MPW1K/6-31+(d) gas phase optimizations give structures close enough to experiment for reliable NMR shielding calculations. Relativistic spin–orbit effects are large for chlorosilane systems and reliable shielding calculations thus require SO corrections for these systems. For non-halosilane systems the SO effects are rather small and ^{29}Si shift predictions are thus possible without any relativistic corrections. Solvent effects on ^{29}Si NMR chemical shifts are quite systematic, but only of moderate size, and reliable shift predictions can thus be made using gas phase geometries and, in many cases, also using gas phase shielding calculations. For the (chloro)organosilane compound family studied here MPW1K/IGLO-III(+ZORA-SO)//MPW1K/6-31+G(d) calculations are thus recommended for ^{29}Si NMR shift calculation.

Computational details

Chemical shifts of ^{29}Si containing species (δ(^{29}Si)) are calculated using eqn (1), where σ(^{29}Si$_{TMS}$) is the chemical shielding for the reference compound tetramethylsilane (Si(CH$_3$)$_4$, TMS, **1**) and σ(^{29}Si) is the shielding of the ^{29}Si nucleus in the compound under investigation:

$$\delta(^{29}\mathrm{Si}) = \sigma(^{29}\mathrm{Si}_{\mathrm{TMS}}) - \sigma(^{29}\mathrm{Si}) \quad (1)$$

Shieldings are calculated using the Gauge-Independent Atomic Orbital (GIAO) method.[58] Shielding values of chemicals are calculated with Gaussian 09, revision C.01[59] and MOLPRO, Version 2012.1.[60,61]

The relativistic spin–orbit corrections to the nuclear magnetic shielding constants for ^{29}Si were calculated with the two-component zeroth-order regular approximation (ZORA)[51,52] using the Amsterdam Density Functional (ADF 2013.01) code.[62] The hybrid functional PBE0[63–65] in combination with the Slater-type basis set TZ2P[66] optimized for relativistic ZORA calculations is used for these single point calculations at MPW1K/6-31+G(d) gas phase structures. The spin–orbit correction is calculated as δ(^{29}Si)$_{ZORA}$–δ(^{29}Si)$_{non\text{-}relativistic}$ and then Boltzmann-averaged for compounds with more than one conformer. For more details on different functionals and basis sets see the ESI.†

Experimental details

All commercial chemicals were of reagent grade and were used as received unless otherwise noted. The substances *tert*-butyldimethylsilyl cyanide (**4**), *tert*-butyldiphenylsilyl chloride (**8**), 1-(*tert*-butyldimethylsilyl)imidazole (**11**), *N*-*tert*-butyldimethylsilyl-*N*-methyltrifluoroacetamide (**16**), and triisopropylsilyl chloride (**20**), were purchased in the highest purity from Sigma Aldrich and measured in freshly distilled $CDCl_3$ over CaH_2. ^{1}H and ^{13}C NMR spectra were recorded on Varian 300 or Varian INOVA 400 machines at room temperature. All ^{1}H chemical shifts are reported in ppm (δ) relative to $CDCl_3$ (+7.26); ^{13}C chemical shifts are reported in ppm (δ) relative to $CDCl_3$ (+77.16). All other

chemicals were purchased from commercial suppliers at the highest available grade, store over orange gel in an desiccator and used without any further purification.

General procedure 1

For all purchased substances this procedure was performed. In a pre-dried NMR tube 30 mg of the substance were dissolved in 0.6 mL of freshly distilled $CDCl_3$. The tube was closed with a cap and sealed with parafilm.

General procedure 2

For the ion pairs (**18**, **19**, **23**, **24**) two stock solutions have been prepared in the concentration of 0.5 M in freshly distilled $CDCl_3$. Both solutions (Lewis base and TBSOTf) are mixed in a ratio 1 : 1 and therefore the concentration of the intermediates can be 0.25 M max. The tube was closed with a cap and sealed with parafilm.

General procedure 3 (silylation of alcohols)

One equivalent of alcohol and 1.2 equivalents of used silyl chloride were dissolved in 20 mL DCM and 1.2 equivalents triethylamine was added. After adding up to 30 mmol% of a catalyst DMAP the reaction mixture stirred at RT up to 7 d. The reaction mixture was washed with sat. aq. NH_4Cl solution, extracted three times with DCM (10 mL) and the combined organic phases dried over $MgSO_4$. The solvent was removed under reduced pressure and column chromatography was used to purify the product.

References

1 T. M. Alam and M. Henry, *Phys. Chem. Chem. Phys.*, 2000, **2**, 23–28.
2 C. van Wüllen, *Phys. Chem. Chem. Phys.*, 2000, **2**, 2137–2144.
3 U. Herzog, *J. Prakt. Chem.*, 2000, **342**, 379–388.
4 X. Xue and M. Kanzaki, *Phys. Chem. Miner.*, 1998, **26**, 14–30.
5 J. A. Tossell and P. Lazzeretti, *J. Chem. Phys.*, 1986, **84**, 369–374.
6 D. H. Brouwer, *J. Magn. Reson.*, 2008, **194**, 136–146.
7 D. Auer, M. Kaupp and C. Strohmann, *Organometallics*, 2004, **23**, 3647–3655.
8 C. Corminboeuf, T. Heine and J. Weber, *Chem. Phys. Lett.*, 2002, **357**, 1–7.
9 M. Profeta, F. Mauri and C. J. Pickard, *J. Am. Chem. Soc.*, 2003, **125**, 541–548.
10 J. Casanovas, F. Illas and G. Pacchioni, *Chem. Phys. Lett.*, 2000, **326**, 523–529.
11 R. Herges and F. Starck, *J. Am. Chem. Soc.*, 1996, **118**, 12752–12757.
12 J. Ambati and S. E. Rankin, *J. Phys. Chem. A*, 2010, **114**, 5279–5286.
13 T. Heine, A. Goursot, G. Seifert and J. Webert, *J. Phys. Chem. A*, 2001, **105**, 620–626.
14 A. I. Poblador-Bahamonde, R. Poteau, C. Raynaud and O. Eisenstein, *Dalton Trans.*, 2011, **40**, 11321–11326.
15 F. Meyer-Wegner, A. Nadj, M. Bolte, N. Auner, M. Wagner, M. C. Holthausen and H. W. Lerner, *Chem. – Eur. J.*, 2011, **17**, 4715–4719.
16 M. Karni, Y. Apeloig, N. Takagi and S. Nagase, *Organometallics*, 2005, **24**, 6319–6330.
17 M. Suginome and Y. Ito, *Chem. Rev.*, 2000, **100**, 3221–3256.
18 R. P. Singh and J. M. Shreeve, *Tetrahedron*, 2000, **56**, 7613–7632.
19 P. Patschinski, C. Zhang and H. Zipse, unpublished results.
20 B. J. Lynch, P. L. Fast, M. Harris and D. G. Truhlar, *J. Phys. Chem. A*, 2000, **104**, 4811–4815.
21 A. F. Wallace, G. V. Gibbs and P. M. Dove, *J. Phys. Chem. A*, 2010, **114**, 2534–2542.
22 A. D. Boese and N. C. Handy, *J. Chem. Phys.*, 2001, **114**, 5497.
23 V. A. Du, G. N. Stipicic and U. Schubert, *Eur. J. Inorg. Chem.*, 2011, 3365–3373.
24 Y. Zhao, N. E. Schultz and D. G. Truhlar, *J. Chem. Theory Comput.*, 2006, **2**, 364–382.
25 Y. Zhao and D. G. Truhlar, *Theor. Chem. Acc.*, 2007, **120**, 215–241.
26 B. Maryasin and H. Zipse, *Phys. Chem. Chem. Phys.*, 2011, **13**, 5150–5158.
27 S. Sklenak, J. Dědeček, C. Li, B. Wichterlová, V. Gábová, M. Sierka and J. Sauer, *Phys. Chem. Chem. Phys.*, 2009, **11**, 1237–1247.
28 E. V. van den Berghe and G. P. van der Kelen, *J. Organomet. Chem.*, 1973, **59**, 175–187.
29 M. Tobisu, Y. Kita, Y. Ano and N. Chatani, *J. Am. Chem. Soc.*, 2008, **130**, 15982–15989.
30 K. Ohmatsu, Y. Hamajima and T. Ooi, *J. Am. Chem. Soc.*, 2012, **134**, 8794–8797.
31 B. J. Albert and H. Yamamoto, *Angew. Chem., Int. Ed.*, 2010, **49**, 2747–2749.
32 J. R. Durig, Y. S. Li and R. O. Carter, *J. Mol. Spectrosc.*, 1972, **44**, 18–31.
33 R. C. Mockler, J. H. Bailey and W. Gordy, *J. Chem. Phys.*, 1953, **21**, 1710–1713.
34 P. W. Allen and L. E. Sutton, *Acta Crystallogr.*, 1950, **3**, 46–72.
35 R. Gajda, K. Dziubek and A. Katrusiak, *Acta Crystallogr., Sect. B: Struct. Sci.*, 2006, **62**, 86–93.
36 J. Buschmann, D. Lentz, P. Luger and M. Rottger, *Acta Crystallogr., Sect. C: Cryst. Struct. Commun.*, 2000, **56**(Pt 1), 121–122.
37 F. Weigend, *Phys. Chem. Chem. Phys.*, 2006, **8**, 1057–1065.
38 F. Weigend and R. Ahlrichs, *Phys. Chem. Chem. Phys.*, 2005, **7**, 3297–3305.
39 T. H. Dunning, *J. Chem. Phys.*, 1989, **90**, 1007.
40 W. Kutzelnigg, U. Fleischer and M. Schindler, in *NMR Basic Principles and Progress*, ed. P. Diehl, E. Fluck, H. Günther, R. Kosfeld and J. Seelig, Springer, Berlin/Heidelberg, 1991, vol. 213, pp. 165–262.
41 F. Jensen, *J. Chem. Theory Comput.*, 2008, **4**, 719–727.
42 A. D. Boese and N. C. Handy, *J. Chem. Phys.*, 2001, **114**, 5497–5503.
43 H.-J. Werner, F. R. Manby and P. J. Knowles, *J. Chem. Phys.*, 2003, **118**, 8149.

44 Y. Zhao and D. G. Truhlar, *Theor. Chem. Acc.*, 2008, **120**, 215–241.
45 H. Nakatsuji, T. Nakajima, M. Hada, H. Takashima and S. Tanaka, *Chem. Phys. Lett.*, 1995, **247**, 418–424.
46 T. Helgaker, S. Coriani, P. Jørgensen, K. Kristensen, J. Olsen and K. Ruud, *Chem. Rev.*, 2012, **112**, 543–631.
47 M. Kaupp, O. L. Malkina, V. G. Malkin and P. Pyykkö, *Chem. – Eur. J.*, 1998, **4**, 118–126.
48 A. Bagno, M. Bonchio and J. Autschbach, *Chem. – Eur. J.*, 2006, **12**, 8460–8471.
49 L. A. Truflandier, E. Brendler, J. Wagler and J. Autschbach, *Angew. Chem., Int. Ed.*, 2011, **50**, 255–259.
50 J. Autschbach, K. Sutter, L. A. Truflandier, E. Brendler and J. Wagler, *Chem. – Eur. J.*, 2012, **18**, 12803–12813.
51 E. v. Lenthe, E. J. Baerends and J. G. Snijders, *J. Chem. Phys.*, 1993, **99**, 4597–4610.
52 S. K. Wolff, T. Ziegler, E. van Lenthe and E. J. Baerends, *J. Chem. Phys.*, 1999, **110**, 7689.
53 V. G. Malkin, O. L. Malkina and D. R. Salahub, *Chem. Phys. Lett.*, 1996, **261**, 335–345.
54 Taking ion pair system **19** as an example, the SO correction for the six different conformers shown in Fig. 5 vary from −0.3 to −0.5 ppm at ZORA-SO-PBE0/TZ2P level. After Boltzmann averaging, the SO correction amounts to −0.5 ppm, which is identical to the value of the most stable conformer **19_1** (see ESI† for details).
55 B. Wrackmeyer, C. Stader and H. Zhou, *Spectrochim. Acta, Part A*, 1989, **45**, 1101–1111.
56 NBO calculations were performed using the NBO 3.1 program as implemented in the Gaussian 09 C.01 package.
57 This type of geometry is also obtained upon geometry optimization at MP2(FC)/6-31+G(d) level.
58 R. Ditchfied, *Mol. Phys.*, 1974, **27**, 789–807.
59 M. J. Frisch, G. W. Trucks, H. B. Schlegel, G. E. Scuseria, M. A. Robb, J. R. Cheeseman, G. Scalmani, V. Barone, B. Mennucci, G. A. Petersson, H. Nakatsuji, M. Caricato, X. Li, H. P. Hratchian, A. F. Izmaylov, J. Bloino, G. Zheng, J. L. Sonnenberg, M. Hada, M. Ehara, K. Toyota, R. Fukuda, J. Hasegawa, M. Ishida, T. Nakajima, Y. Honda, O. Kitao, H. Nakai, T. Vreven, J. A. Montgomery, Jr., J. E. Peralta, F. Ogliaro, M. Bearpark, J. J. Heyd, E. Brothers, K. N. Kudin, V. N. Staroverov, T. Keith, R. Kobayashi, J. Normand, K. Raghavachari, A. Rendell, J. C. Burant, S. S. Iyengar, J. Tomasi, M. Cossi, N. Rega, J. M. Millam, M. Klene, J. E. Knox, J. B. Cross, V. Bakken, C. Adamo, J. Jaramillo, R. Gomperts, R. E. Stratmann, O. Yazyev, A. J. Austin, R. Cammi, C. Pomelli, J. W. Ochterski, R. L. Martin, K. Morokuma, V. G. Zakrzewski, G. A. Voth, P. Salvador, J. J. Dannenberg, S. Dapprich, A. D. Daniels, Ö. Farkas, J. B. Foresman, J. V. Ortiz, J. Cioslowski and D. J. Fox, Gaussian, Inc., Wallingford, CT, 2010.
60 H.-J. Werner, P. J. Knowles, G. Knizia, F. R. Manby and M. Schütz, *Wiley Interdiscip. Rev.: Comput. Mol. Sci.*, 2012, **2**, 242–253.
61 H.-J. Werner, P. J. Knowles, G. Knizia, F. R. Manby, M. Schütz and others, see also http://www.molpro.net.
62 ADF2013, SCM, Theoretical Chemistry, Vrije Universiteit, Amsterdam, Netherlands; see also: http://www.scm.com.
63 M. Ernzerhof and G. E. Scuseria, *J. Chem. Phys.*, 1999, **110**, 5029–5036.
64 C. Adamo and V. Barone, *J. Chem. Phys.*, 1999, **110**, 6158–6170.
65 C. Adamo and V. Barone, *J. Chem. Phys.*, 1998, **108**, 664–675.
66 E. van Lenthe and E. J. Baerends, *J. Comput. Chem.*, 2003, **24**, 1142–1156.